



**HAL**  
open science

## Analysis of red-luminescence lifetime components of non-bridging oxygen hole centers in $\gamma$ -ray irradiated silica glasses

Jingang Wang, Jimeng Cheng, Chongyun Shao, Wei Chen, Chunlei Yu, Lili Hu, Malgorzata Guzik, Georges Boulon

### ► To cite this version:

Jingang Wang, Jimeng Cheng, Chongyun Shao, Wei Chen, Chunlei Yu, et al.. Analysis of red-luminescence lifetime components of non-bridging oxygen hole centers in  $\gamma$ -ray irradiated silica glasses. *Optical Materials Express*, 2023, 13 (12), pp.3616. 10.1364/OME.506661 . hal-04390021

**HAL Id: hal-04390021**

**<https://hal.science/hal-04390021>**




Submitted on 12 Jan 2024

**HAL** is a multi-disciplinary open access archive for the deposit and dissemination of scientific research documents, whether they are published or not. The documents may come from teaching and research institutions in France or abroad, or from public or private research centers.

L'archive ouverte pluridisciplinaire **HAL**, est destinée au dépôt et à la diffusion de documents scientifiques de niveau recherche, publiés ou non, émanant des établissements d'enseignement et de recherche français ou étrangers, des laboratoires publics ou privés.



# Analysis of red-luminescence lifetime components of non-bridging oxygen hole centers in $\gamma$ -ray irradiated silica glasses

JINGANG WANG,<sup>1,2</sup>  JIMENG CHENG,<sup>1</sup> CHONGYUN SHAO,<sup>1</sup> WEI CHEN,<sup>1,5</sup>  CHUNLEI YU,<sup>1</sup> LILI HU,<sup>1</sup>  MALGORZATA GUZIK,<sup>3</sup> AND GEORGES BOULON<sup>4,6</sup>

<sup>1</sup>Key Laboratory of Materials for High Power Laser, Shanghai Institute of Optics and Fine Mechanics, Chinese Academy of Sciences, Shanghai 201800, China

<sup>2</sup>Center of Materials Science and Optoelectronics Engineering, University of Chinese Academy of Sciences, Beijing 100049, China

<sup>3</sup>University of Wrocław, Faculty of Chemistry, ul. F. Joliot-Curie 14, 50-383 Wrocław, Poland

<sup>4</sup>University of Lyon, Institute Light Matter (iLM), UMR 5306 CNRS-Claude Bernard/Lyon1 University, 69622 Villeurbanne, France

<sup>5</sup>weichen@siom.ac.cn

<sup>6</sup>georges.boulon@univ-lyon1.fr

**Abstract:** The relation between 1.9 eV red-luminescence intensity of non-bridging oxygen hole centers (NBOHCs) in silica and incident laser shot number was proved to be important to predict the occurrence of laser damage, in which a more precise prediction will benefit from a deeply understanding of the red-luminescence of NBOHCs. This study focuses on analyzing NBOHCs in silica glasses irradiated by gamma rays, including the electron paramagnetic resonance spectra in the main  $g_2$  factor range, excitation spectra in the UV range, emission spectra and emission lifetimes in the red range, as well as their relations with hydroxyl and temperature. At 53 K, the main  $g_2$ -factor of NBOHCs in high-hydroxyl (high-OH) and low-hydroxyl (low-OH) silica differs by only  $\sim 1.5 \times 10^{-4}$ . Whereas in the higher  $g$ -value side of the main  $g_2$ -factor band, low-OH silica exhibited a little broadened resonance absorption bandwidth. At room temperature, the 5.64-3.44 eV excitation spectra monitoring at 1.9 eV and the 2.16-1.65 eV emission spectra exciting at 4.8 eV exhibit the same excitation peak of 4.54 eV and emission peak of 1.907 eV for both high-OH and low-OH silica. Whereas at liquid-N<sub>2</sub> temperature, high-OH silica exhibits a broader emission bandwidth in the higher energy side of the red-luminescence band. At room temperature, the average emission lifetime of NBOHC in high-OH silica is 14.5  $\mu$ s, whereas that in low-OH silica is 13.4  $\mu$ s. However, at liquid-N<sub>2</sub> temperature, their average lifetimes respectively increased and decreased greatly to 22.3 and 9.7  $\mu$ s, showing a quite obvious variation. In high-OH silica, the large number of hydroxyl attract the hydrogen ions that are released with the temperature decrease, forming metastable hydrogen-bonded hydroxyl. Finally, only NBOHCs corresponding to longer lifetime components, without neighboring hydrogen and its interaction, remain in the high-OH silica at lower temperature. In low-OH silica, there is few hydroxyl, so that the hydrogen released with the temperature decrease can only act on NBOHCs without neighboring hydrogen. Finally, those NBOHCs that correspond to shorter lifetime components and interact with neighboring hydrogen remain in the low-OH silica at lower temperature. The results on the characteristics of this red luminescence provides new ideas and ways for the future prediction about the laser damage of silica. Especially, the component analysis on the emission lifetime decay curves that can reflect the characteristics of NBOHCs and their neighboring environment can not only be used to distinguish between contributions to the red-luminescence from different types of NBOHCs, but also to analyze the relations between other ions or defects around NBOHCs and laser damage initiation, for a more precise prediction.

© 2023 Optica Publishing Group under the terms of the [Optica Open Access Publishing Agreement](#)

## 1. Introduction

Various defects in silica glasses [1] are commonly regarded as precursors to the laser induced damage, since they are closely but intricately related to laser induced damage thresholds [2]. With the occurrence of laser induced damage, a variety of luminescence bands in a very broad spectral range from ultraviolet to visible are generated for silica glasses [3], corresponding to the generation of various defects. Among these, non-bridging oxygen hole centers (NBOHCs) are relatively sensitive, and their concentration increases by 1–2 orders of magnitude after laser damage [4]. Unlike surface indentations, only at laser induced damage sites, the 1.9 eV red luminescence of NBOHCs in silica can be observed [5]. Especially, the peak intensity of the red luminescence increases with the number of nanosecond laser pulses [6]. Such a highly significant relation has been applied to predict the laser induced damage of silica under multi-pulse laser operating conditions [6], in which the key is how to understand the components of the red luminescence of NBOHCs. Under the nanosecond laser conditions, more accurately predicting the occurrence of laser induced damage for large-sized silica optical elements has significant implications for the ongoing operation of the National Ignition Facility in USA [7], the Laser Megajoule facility in France [8] and the ShenGuang facility in China [9].

High power laser systems such as Extreme Light Infrastructure (ELI) have advanced to femtosecond regimes [10]. The investigation on the interaction between lasers and materials such as silica glasses under femtosecond pulse conditions holds significant value in terms of fundamental researches and practical applicabilities [11–14]. When subjected to femtosecond laser irradiation, the red luminescence from NBOHCs can be detected even within nonmelted regions, but this luminescence phenomenon is unstable [11]. Therefore, an investigation on the luminescence characteristics of defects is imperative because the insights offered by these defect characteristics can significantly advance the understanding of the interaction between silica glasses and lasers [11]. Even the defect characteristics existing before the laser induced damage can be correlated with the laser induced damage resistance exhibited by silica glass optical components. The red luminescence from NBOHCs can be used to study the effect of ion beam sputtering polishing of silica glasses on laser induced damage [15] and can also be used to analyze laser damaging precursors distributed near the surface of silica glass [16].

Whether as possible laser damage precursors [6] or as final products of laser irradiation [11], their existence and evolution of NBOHCs are unstable [6,11]. Especially, the emission peak and lifetime reported in the literatures for such a red luminescence band of NBOHCs in silica glasses are somewhat different [17–19], with a certain degree of uncertainty. Therefore, it is necessary to study the characteristics of the red luminescence of NBOHCs for predicting the laser induced damage of silica glasses in advance, and also for analyzing and judging the internal quality and processing technology for silica glass optical components. In this study, the gamma-ray irradiation induced NBOHCs in ultra-high purity synthetic silica glasses with high and low hydroxyl group contents are analyzed. They are of the same red luminescence as that of NBOHCs induced by laser irradiation [5], but with a stable and suitable content due to a controlled low and high dose gamma-ray irradiation, which is beneficial to analyze and characterize NBOHCs. And the results obtained from gamma ray induced NBOHCs can also apply to those induced by laser irradiation, which must be helpful for the future prediction about the laser induced damage of silica. Section 3.1 focuses on the analysis of the electron paramagnetic resonance spectra. Section 3.2 focuses on the analysis of the excitation and the emission spectra. Section 3.3 focuses on the analysis of the emission lifetime decay curves. Based on the results in section 3.1 and 3.2, section 3.4 discusses the longer and shorter lifetime components deduced from the emission lifetime decay curves in section 3.3, which are related to the alteration of two types of NBOHCs with and without neighboring hydrogen ions and their interaction.

## 2. Experimental

Two samples of ultra-high purity silica by flame hydrolysis were applied in this study, with hydroxyl contents of 7 ppm and 425 ppm, respectively named as low-OH and high-OH silica. Fourier transform infrared (FTIR) spectrometer, Nicolet 6700, was used to determine the hydroxyl content in silica. Except for the hydroxyl, the total impurity content in both low-OH and high-OH silica is smaller than 5 ppm, which was determined by the inductively coupled plasma optical emission and mass spectrometers, Thermo Fisher ICAP 6300 and ICP-MS TQ.

After cutting and polishing to  $50 \times 50 \times 5$  mm, the samples were irradiated twice with a  $^{60}\text{Co}$  gamma-ray radiation source, respectively with total doses of 0.005 MGy and 0.5 MGy, by using the radiation dose rate of 29.4 kGy/h.

Electron paramagnetic resonance (EPR) spectra were determined by using Bruker E580 ELEXSYS instrument operating in the X-band of  $\sim 9.38$  GHz. The magnetic field range is from 3300 to 3400 G. The microwave power is 0.47 mW. The scan time is set to 20 seconds, with the resolution of 2048 data points over 200 Gauss range.

Excitation spectra, emission spectra, and emission lifetime decay curves were recorded using Edinburgh FLS920 steady-state and transient fluorescence spectrometer. A 450 W Xe2 continuous-wave Xenon lamps was used to determine the emission spectra in the range of 575–750 nm (2.16–1.65 eV) and the excitation spectra in the range of 220–360 nm (5.64–3.44 eV). A 60 W  $\mu\text{F}2$  pulsed Xenon lamp and a microchannel plate photomultiplier tube R3809U-50 detector were used to determine 650 nm (1.9 eV) emission lifetime decay curves.

## 3. Results and discussion

### 3.1. EPR spectra of NBOHC in low-OH and high-OH silica glasses

Electron paramagnetic resonance technology has a high sensitivity to detect low paramagnetic defect contents, and its detection limit can be as low as  $10^{14}$  spins/cm<sup>3</sup> [20]. The EPR spectra of the NBOHCs recorded for low-OH and high-OH silica glasses irradiated with a small dose of 0.005 MGy gamma rays are shown in Figs. 1(a) and 1(b), respectively. Owing to Curie's law, which indicates that the paramagnetic susceptibility of a material is inversely proportional to temperature, it is generally not easy to detect the paramagnetic signal of NBOHCs in silica at room temperature [21]. In particular, when the contents of NBOHC generated under low dose irradiation is lower, the two spectra measured at room temperature, as shown in Figs. 1(a) and 1(b), do not exhibit any effective signals of NBOHC paramagnetic defects.

As the temperature drops below the liquid-N<sub>2</sub> temperature region, the paramagnetic signal of NBOHC has been highlighted. In X-band EPR spectra, the paramagnetic signal located in 3330–3340 G range belongs to the  $g_2$  factor among the three main  $g$  factors of NBOHC. Its  $g_1$  factor located at the higher magnetic field overlaps with the  $g$  factor of silicon dangling bond E' defect [22]. And its  $g_3$  factor located at the lower magnetic field cannot be observed even at low temperature [23]. It is mainly because the  $g_3$  factor broadening phenomenon for NBOHC in silica is relatively significant, and its width can reach five times that of the peroxy radical defect in silica [24]. And the content of NBOHC is lower than four times [24] or six times [25] of the peroxy radical defect. Thus, it is difficult to characterize NBOHCs with its  $g_3$  factor.

In the spectra for the  $g_2$  factor of NBOHCs, as in Fig. 1, no intensity correction is made by the temperature factor related to Curie's law. The comparison between Figs. 1(a) and 1(b) in the same temperature range, about 20–40 K below the liquid-N<sub>2</sub> temperature, shows that the paramagnetic signal of the high-OH silica is significantly stronger than that of the low-OH silica. Whether or not there occurs EPR-silent phenomenon that some of NBOHCs in silica do not produce EPR signal [21], if assuming the silent proportions of NBOHCs are the same in both silica, the content of NBOHCs in high-OH silica is greatly higher by a factor of three or more than that in low-OH silica, in the case of low dose irradiation of 0.005 MGy. But in the case of

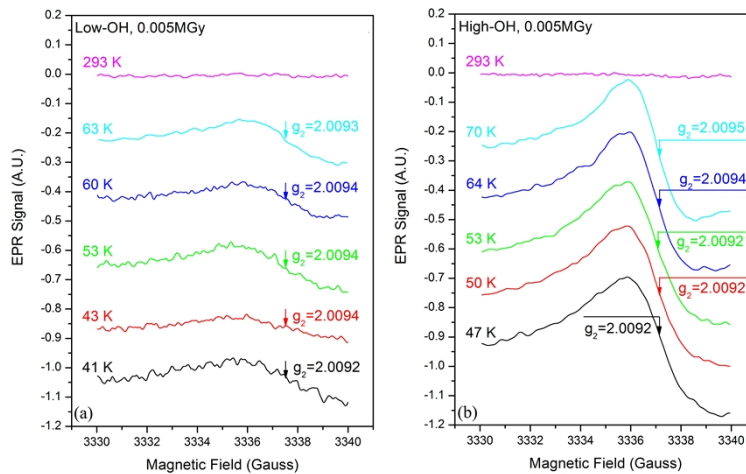


**Fig. 1.** Room-temperature and low-temperature EPR spectra of NBOHC in (a) low-OH and (b) high-OH silica glasses after irradiation with 0.005MGy gamma rays.

0.5 MGy high dose, the content of NBOHC in high-OH silica is only two times higher than that in low-OH, according to the excitation and emission spectra as shown in the following section 3.2. However, since there exist more EPR-silent NBOHCs in dry (low-OH) silica [21], the content ratio of three or more is overestimated by the EPR spectra in Fig. 1. It should be consistent with the content ratio of two estimated by the excitation and emission spectra, thus implying that the NBOHCs do not change with the irradiation dose. As for the mechanism and condition of the EPR-silent for NBOHCs are still not so clear [21].

For the NBOHCs that produce paramagnetic signal, either in low-OH silica as in Fig. 1(a), or in high-OH silica as in Fig. 1(b), the  $g_2$  values remain within the range of 2.0092–2.0095. These values are close to  $g_2 = 2.01$  of NBOHC induced by  $\gamma$ -ray irradiation [26] or silver-ion bombardment [27]. For the NBOHCs resulting from fiber-drawn [28], introduced by fluoride ions [29], and produced in mesoporous silica glass [30], their  $g_2$  factors are greatly increased, being 2.0111, 2.0109, and 2.0115, respectively. To some extent, these situations reflect that the silica glasses determined in Fig. 1 should be high-purity and high-quality silica. If we only consider the value of the  $g_2$  factor, the internal structure of the NBOHCs in the low-OH silica glass should be equal to that in the high-OH silica glass.

To further compare the EPR characteristics of NBOHCs in the silica glasses with different hydroxyl contents, the two resonance spectra at 53 K in Figs. 1(a) and 1(b) are normalized as shown in Fig. 2. Close to the high magnetic field of 3337 G, the  $g_2$  values of the NBOHCs in low-OH and high-OH silica glasses differ only by  $\sim 1.5 \times 10^{-4}$ . But close to the low magnetic field region of 3335 G, the difference in the  $g_2$  values of the two centers increases to  $6.7 \times 10^{-4}$ . Although this region does not represent the peak region of the  $g_2$  band, it reflects an observed shrinkage does occur in the high  $g$ -value region of the  $g_2$  factor resonance absorption band of NBOHCs in high-OH silica, compared with that in low-OH silica. The low-OH silica exhibits a little broader spectrum in the high  $g$ -value region of the  $g_2$  factor resonance absorption band. Such a bandwidth difference will be more pronounced in the integrated EPR spectra. It can be argued that, although the main  $g_2$  factor values of NBOHCs do not change fundamentally, the bandwidth of the  $g_2$  factor resonance absorption band does change, which should be related to the surrounding environments around NBOHCs, as discussed in the following Section 3.4.

To clarify the possible reasons for this change, fluorescence detection was used, but this required a further increase in the contents of NBOHCs in silica glasses. After increasing the

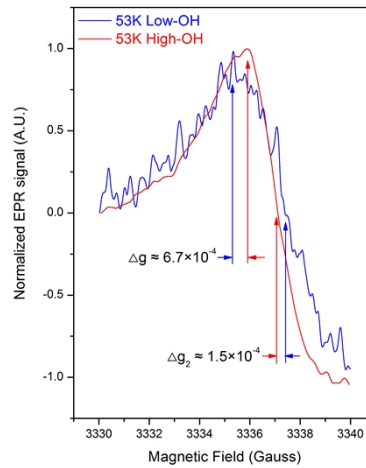


**Fig. 2.** Normalized EPR spectra of NBOHC in low-OH and high-OH silica glasses at 53 K, redepicted by the two 53 K spectra of Fig. 1 (a) and (b)

gamma ray irradiation dose to 0.5 MGy, the low-OH silica has exhibited an EPR signal at room temperature, although the signal-to-noise ratio is not high enough, as shown in Fig. 3. At this time, the room temperature resonance signal of the high-OH silica is quite obvious as shown in Fig. 3, and especially the main  $g_2$  factor still remains to be 2.0095, equal to the  $g_2$  factors in the case of low irradiation dose, as shown in Fig. 1 (a) and (b). This indicates that NBOHCs do not fundamentally change with the irradiation dose from 0.005 to 0.5 MGy, and their content also increases to a level that can be used for fluorescence detection.

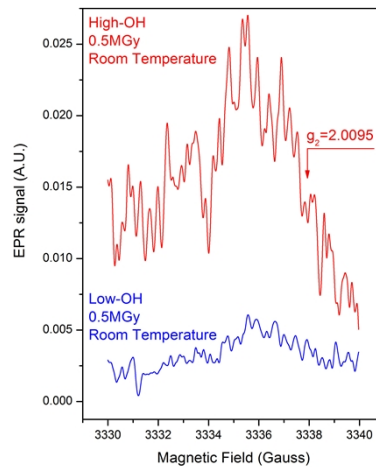


**Fig. 3.** EPR spectra of NBOHC in low-OH and high-OH silica glasses irradiated with 0.5MGy gamma rays at room temperature.

### 3.2. Excitation and emission spectra of NBOHC in high-OH and low-OH silica glasses

Both the red luminescence band located at 1.9 eV [17] and the broad absorption band located near 4.8 eV were confirmed to belong to NBOHCs in silica [17,26]. The position of this UV absorption band is close to that 5.8 eV absorption band [31] of the silicon dangling bond with an unpaired electron, and the two bands overlap. Although the absorption of silicon dangling bond is

generally more stronger, it does not show any emission [32]. In the excitation spectra monitoring the 1.9 eV red luminescence, the 4.8 eV UV region is not disturbed and only the excitation band belonging to NBOHCs exists. Figure 4 shows the excitation spectra of the high-OH and low-OH silica, for the red luminescence of NBOHCs. They are generally consistent with the induced absorption spectra of NBOHCs [17]. The room-temperature excitation peak is about 0.2 eV lower than the induced absorption peak [17], and about 0.1 eV higher than the excitation peak [33] of the NBOHCs generated by near-infrared femtosecond-laser irradiation. Same as the reported [5], these facts again indicate that the NBOHCs induced by gamma-ray irradiation are the same as those induced by laser irradiation. The excitation peak of high-OH silica shifts slightly from  $\sim 4.54$  eV at room temperature to  $\sim 4.56$  eV at liquid-N<sub>2</sub> temperature, while that of low-OH silica shifts slightly from  $\sim 4.54$  eV at room temperature to  $\sim 4.59$  eV at liquid-N<sub>2</sub> temperature, as shown in Fig. 4. The general trend is that the performances of the high-OH and low-OH silica are the same at room temperature, whereas at lower temperatures the excitation peak values of them are slightly different. Overall, the effects of temperature on the peak and bandwidth of the excitation spectra are not apparent. However, as in Fig. 4, the intensity clearly exhibits a temperature effect that increases as the temperature decreases.

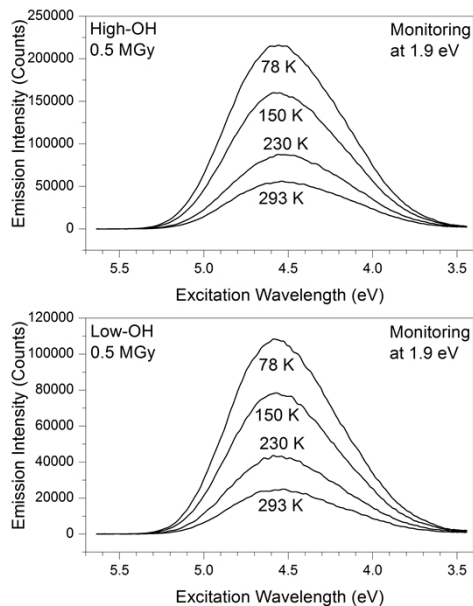


**Fig. 4.** Excitation spectra of NBOHC in high-OH and low-OH silica glasses after irradiation with 0.5 MGy gamma rays, from liquid-N<sub>2</sub> temperature to room temperature.

Correspondingly, the intensity of the red luminescence of NBOHCs also clearly exhibits a temperature effect that increases with decreasing temperature. As shown in Fig. 5, both high-OH and low-OH silica exhibits the emission spectra from 1.65 to 2.15 eV, excited at 4.8 eV. In contrast to the excitation spectra, as the temperature decreases, the peak of the emission band shifts from high to low energy, with a red-shift. To be exact, the emission peak of the high-OH silica decreases slightly from  $\sim 1.907$  eV at room temperature to  $\sim 1.881$  eV at liquid N<sub>2</sub> temperature, while that of the low-OH silica glass decreases slightly from  $\sim 1.907$  eV at room temperature to  $\sim 1.876$  eV at liquid N<sub>2</sub> temperature. The general trend is still that the performances of the high-OH and low-OH silica are the same at room temperature, whereas their peak values are slightly changed at low temperature. What should be noted is the reasons resulting in such a change. The change in the peak values of the red luminescence bands with temperature decrease,

as in Fig. 5, is accompanied by the red-shift of the entire emission band to the lower energy region. There is almost no observed change in the bandwidth and spectral lineshape, including the broadening or the narrowing with temperature decrease. If there is a strong electron–phonon coupling, the bandwidth of the red luminescence should broaden by  $\sim 0.04$  eV as the temperature increases [34]. According to the analysis of the zero-phonon line of the red-luminescence of NBOHCs in silica, the electron–phonon coupling interaction is not strong. The maximum Huang–Rhys factor is  $\sim 3.2$  [34], and it might even be  $< 1.5$  [19]. This indicates that the interaction between the NBOHCs and the surrounding matrix is not strong, although in silica, there exists an evident coupling interaction between the two-coordinated Si or Ge defects and the surrounding matrix [34]. Therefore, the above-mentioned change in the peak value of the red luminescence with temperature decrease cannot be attributed to the electron–phonon coupling. There may also be other important reason for such a change. On the other hand, regarding the comparison between the high-OH and low-OH silica, it is found that the high-OH silica exhibits a slight but obvious broadening at the end of higher energy side of the red luminescence. But it only can appear at liquid N<sub>2</sub> temperature, similar to the reported red luminescence behavior of dry and wet silica at liquid He temperature [34]. This broadening seems to be related to the excitation wavelength for the red luminescence [34]. However, just like the possible reasons resulting in the above-mentioned change in the peak value, other reasons may also be considered for such a broadening. Both two phenomena can also be related with the surrounding environment close to NBOHCs in silica, according to the following discussion in Section 3.4.

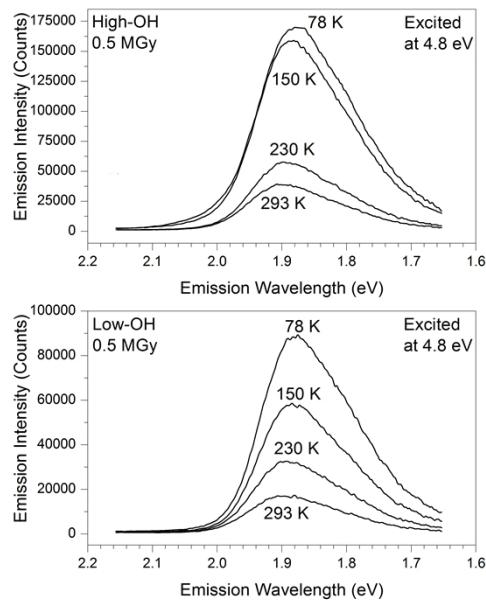


**Fig. 5.** Emission spectra of NBOHC in high-OH and low-OH silica glasses after irradiation with 0.5 MGy gamma rays, from liquid-N<sub>2</sub> temperature to room temperature.

The EPR spectra in Section 3.1, as well as the excitation spectra and the emission spectra in this section, they all exhibit a special temperature effect. It is that the high-OH and low-OH silica glasses behave almost the same at room temperature, but at low temperature they show a slight but obvious difference. Such a difference is more significant in the emission lifetime decay curves of the red luminescence of NBOHCs, as described in the following sections.



### 3.3. Emission lifetime decay curves of NBOHC in high-OH and low-OH silica glasses

Figures 6(a) and (b) show the emission lifetime decay curves of the 1.9 eV red luminescence of NBOHCs in the high-OH and low-OH silica, respectively. At 293 K, all the emission decay curves deviate from the single exponential form at least to a certain extent [17]. As for the average emission lifetime, as the characteristic value of the red luminescence decay, it is not a definite value but is distributed in the range of 10–15  $\mu\text{s}$  [17]. The degree deviating from the single exponential decay form, and the experimental values of the average emission lifetime, they seem to depend on the specific silica glass materials and irradiation methods. However, there are no reports on the relevant variation regularity for the emission lifetime of the red luminescence. When the emission lifetime decay curve is described in the single exponential form, the lifetime can be 12  $\mu\text{s}$  [35], 17  $\mu\text{s}$  [36], 14  $\mu\text{s}$  [37], and 15  $\mu\text{s}$  [38]. However, by observing the decay curves, they are not in the form of a purely single exponential decay. Some deviate from the single exponential form [35,37] at the initial decay stage, whereas others deviate from the single exponential form [36,38] at final decay stage. A more reasonable postulation for the lifetime decay form of the red luminescence of NBOHCs should be a multi-exponential decay form with characteristic decay lifetimes between 10 and 40  $\mu\text{s}$  [39]. A shorter emission lifetime of 10.2  $\mu\text{s}$  [40] was reported for the red luminescence of NBOHCs in silica, generated after electron irradiation. A longer emission lifetime of 41.2  $\mu\text{s}$  [41] was reported for the red luminescence of NBOHCs on silica surface, generated by oxygen adsorption. As shown in Figs. 6(a) and (b), the NBOHCs induced by 0.5MGy gamma-ray irradiation exhibit an average emission lifetime of 14.5  $\mu\text{s}$  for the high-OH silica at room temperature, while the lifetime is 13.4  $\mu\text{s}$  for the low-OH silica. At room temperature, there is a slight but obvious difference between the average emission lifetimes of the high-OH and low-OH silica glasses.

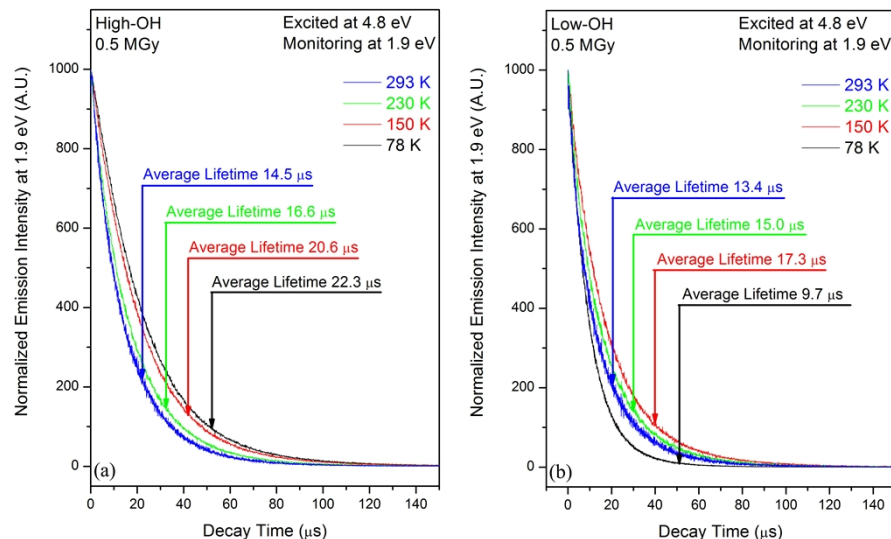


**Fig. 6.** Emission lifetime decay curves of 1.9-eV red luminescence of NBOHC in (a) high-OH and (b) low-OH silica glasses after irradiation with 0.5 MGy gamma rays, from liquid-N<sub>2</sub> temperature to room temperature.

For the high-OH silica, it can be seen in Fig. 6(a) that the average emission lifetime of NBOHCs gradually increases from 14.5  $\mu\text{s}$  at 293 K to 22.3  $\mu\text{s}$  at 78 K as the temperature decreases. On the other hand, as seen in Fig. 6(b), the emission lifetime of the low-OH silica gradually increases from 13.4  $\mu\text{s}$  at 293 K to 17.3  $\mu\text{s}$  at 150 K as the temperature decreases. Whether in high-OH or low-OH silica glasses, the average lifetime of NBOHCs is increased obviously with temperature

decrease, since the non-radiative transition occurring on NBOHCs is suppressed with temperature decrease. However, it should be pointed out that, for the low-OH silica as seen in Fig. 6(b), when the temperature decreases from 150 to 78 K, the average emission lifetime does not increase further, but instead it decreases from 17.3  $\mu\text{s}$  to 9.7  $\mu\text{s}$ . Because the types and forms of various defects in silica are quite complex [17], although no other red emission centers can be found in the EPR spectra of Section 3.1, and in the emission spectra of Section 3.2, the possible influence from this aspect also needs to be considered. A red luminescence band located at 1.85 eV could be produced in silica after high temperature annealing, but its emission lifetime is as longer as about 5 ms [42]. In gamma-ray-irradiated silica, a red luminescence band located at 1.8 eV could also be produced, but its emission lifetime is only about 200 ns [43]. As for another gamma-ray irradiation-induced defects, its emission is at 2.1 eV [44], deviating far away from the studied 1.9 eV red luminescence. Thus, it is believed that the short lifetime of 9.7  $\mu\text{s}$  at 78 K, as shown in Fig. 6(b), really results from the NBOHCs in the low-OH silica.

Seeing that all of the average emission lifetimes as shown in Fig. 6(a) and (b) belong to NBOHCs, the difference between Fig. 6(a) and (b) can be compared. At the same temperature, the average lifetime of the high-OH silica is always longer than that of the low-OH silica. This implies that, if there are two types of NBOHCs, their emission lifetimes must differ. All of the red luminescence decay curves in Figs. 6(a) and (b) are now fitted by using a double exponential function [45]. Both the fitted longer and shorter lifetimes, and their corresponding fitted percentages of each lifetime component to the total amount of NBOHC, are all plotted in Fig. 7 and Fig. 8, respectively illustrating the characteristics of the NBOHCs in the high-OH and low-OH silica glasses, which will be discussed in the following section.

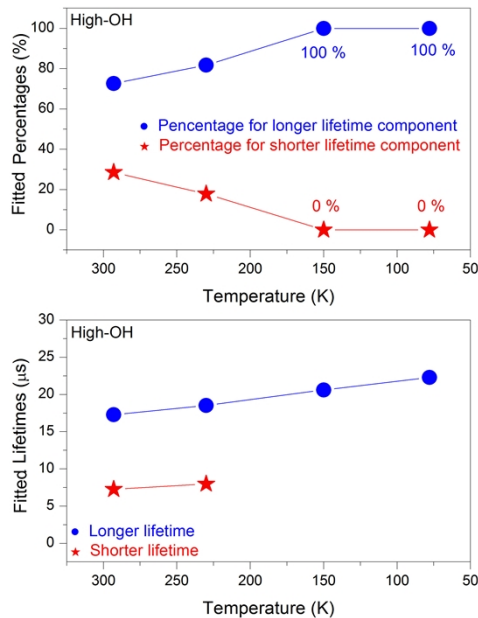


**Fig. 7.** The fitted emission lifetimes (bottom) with longer and shorter components for NBOHCs in high-OH silica glass, and their respective proportions (top) in the total number of NBOHCs.

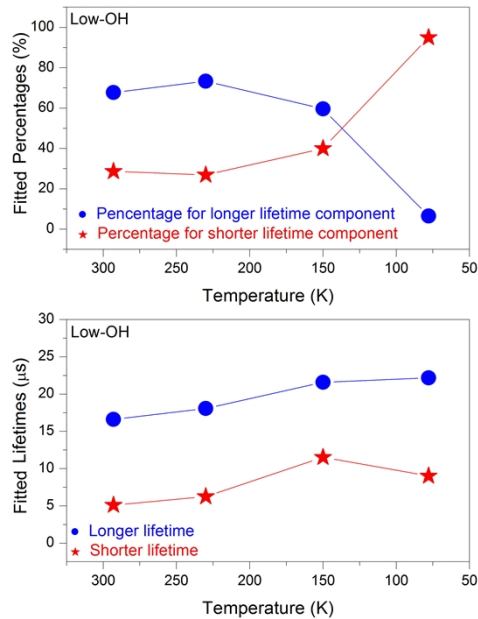


**Fig. 8.** The fitted emission lifetimes (bottom) with longer and shorter components for NBOHCs in low-OH silica glass, and their respective proportions (top) in the total number of NBOHCs.

### 3.4. Long and short lifetime components of NBOHC in high-OH and low-OH silica glasses

Figure 7 shows the relations of the longer and shorter lifetime components, as well as their corresponding percentages of each lifetime component to the total NBOHCs in the high-OH silica, with decreasing the temperature. The longer lifetime increases from 17.3  $\mu\text{s}$  at 293 K to 22.3  $\mu\text{s}$  at 78 K, and its corresponding percentage rises from 72.6% at 293 K to 100% at 150 K and 78 K. On the other hand, the shorter lifetime increases from 7.3  $\mu\text{s}$  at 293 K to 8.0  $\mu\text{s}$  at 230 K. But, as the temperature decreases further from 230 K, the short lifetime component starts to disappear immediately. Figure 7 clearly indicates that, for the high-OH silica, only the longer lifetime component remains at 150 K and 78 K, but meanwhile the shorter lifetime component does not exist at low temperature.

Figure 8 shows the relations of the longer and shorter lifetime components, as well as their corresponding percentages of each lifetime component to the total NBOHCs in the low-OH silica, with decreasing the temperature. The longer lifetime increases from 16.7  $\mu\text{s}$  at 293 K to 22.2  $\mu\text{s}$  at 78 K, whereas its corresponding percentage tends to drop from 150 K to 78 K. Only a very little amount of the longer lifetime component remains at 78 K. On the other hand, the shorter lifetime tends to increase obviously from 5.1  $\mu\text{s}$  at 293 K to 9.0  $\mu\text{s}$  at 78 K, and its corresponding percentage rises from 28.6% at 293 K to 95.0% at 78 K. Figure 8 clearly indicates that, for low-OH silica glass, almost only the shorter lifetime component remains at 78 K, but meanwhile the longer lifetime component does not exist almost fully at 78 K.

Before discussing the reasons that the shorter and longer lifetime components respectively disappear in the cases of the high-OH and low-OH silica glasses, those two relations of the lifetime with temperature decrease are compared firstly, as shown at the bottom of Fig. 7 and Fig. 8. Whether in the high-OH or low-OH silica glasses, there exhibits an increasing trend as the temperature decreases. Although the double exponential fitting cannot exclude the influence of the disordered glass structure, the above trend is completely consistent with the regularity that the

emission lifetime increases because of suppressing the nonradiative transitions with temperature decrease. And especially, the obvious anomaly that the lifetime of 9.7  $\mu\text{s}$  at 78 K is far smaller than the lifetime of 13.4  $\mu\text{s}$  at 293 K as shown in Fig. 6(b) does not occur. This can demonstrate the reasonableness of the double-exponential fitting and its results, which can be used to discuss the reasons that the shorter or longer lifetime components respectively disappear fully or almost fully as the temperature decreases.

Further comparing the two relations of the fitted percentage of longer or shorter lifetime component with temperature decrease, as shown at the top of Fig. 7 and Fig. 8, there are two situations observed. At room temperature, the percentages of longer and shorter lifetime components in the high-OH and low-OH silica are slightly different but basically the same. At low temperature, only the longer component dominates in the high-OH silica, but only the shorter component dominates in the low-OH silica. The combination of these two situations implies that, as the temperature decreases, the shorter component is converted into the longer component in the high-OH silica, and the longer component is converted into the shorter in the low-OH silica. Based on the analysis of the EPR in Section 3.1, as well as the excitation and emission spectra in Section 3.2, such an alteration cannot be an intrinsic transformation of NBOHCs. The internal structure of NBOHCs should not be changed fundamentally. Thus, the alteration of NBOHCs can only be attributed to possible changes surrounding NBOHCs, such as [45] hydroxyl groups or hydroxyl-related factors in the glass network.

As stated above, the percentages of longer and shorter lifetime components in the high-OH and low-OH silica are slightly different but basically the same at room temperature. On the other hand, the hydroxyl contents in the high-OH and low-OH silica differ by an order of magnitude. It indicates that the possible changes surrounding NBOHC should not be hydroxyl.

The hydroxyl contents in the low-OH and high-OH silica are increased after 0.5 MGy  $\gamma$ -ray irradiation, respectively from 7 ppm to 9 ppm and from 425 ppm to 555 ppm, according to the  $3672\text{ cm}^{-1}$  absorption intensities determined by the FTIR spectra [38]. This fact means that there exists additional hydrogen source in silica to form the increased hydroxyl group, since the low-OH and high-OH silica glasses were prepared by flame hydrolysis. During the irradiation, most of these hydrogen atoms are used to form hydroxyl groups, resulting in the increase of the hydroxyl content. On the other hand, there is also a small amount of hydrogen to act upon some NBOHCs during their generation due to the gamma irradiation. Whether in the high-OH or low-OH silica, the periphery surrounding NBOHCs can be distinguished into two cases with the presence or absence of hydrogen in the immediate vicinity of NBOHCs. Since the hydroxyl contents increase greatly during gamma irradiation, most of the precursors to generate NBOHCs are not primarily the hydroxyl Si-OH, but the strained Si-O-Si in silica. Thus, in the high-OH and low-OH silica, most of NBOHCs are without neighboring hydrogen.

Based on the above deduction and the relations between the percentages of the longer and shorter lifetime components and their lifetimes, as shown in Fig. 7 and Fig. 8, the NBOHCs without neighboring hydrogen should correspond to the longer lifetime components. If there emerges hydrogen surrounding NBOHCs, although there is no fundamental change for the energy level structure of NBOHCs, such a hydrogen interaction results in a shorter lifetime since it leads to a more serious nonradiative transition [41].

The identification that the shorter and longer lifetimes respectively correspond to the NBOHCs with the presence and absence of neighboring hydrogen interaction can be further evidenced by the similar surface defects. By subjecting the surface of silica film to chemical adsorptions of hydrogen or oxygen [41], the formed surface NBOHCs bonded with hydrogen have a shorter lifetime of 10.5  $\mu\text{s}$ , whereas the formed surface NBOHCs without hydrogen interaction have a longer lifetime of 41.2  $\mu\text{s}$ .

It should be pointed out that the alteration of two types of NBOHCs with and without existing neighboring hydrogen is not related to the transformation of NBOHCs but to the migration of

hydrogen. If the transformation of NBOHCs occurs, the energy level structure of NBOHCs must be changed. However, as analyzed in Section 3.1, 3.2, there is only a slight change for the EPR spectra, as well as the excitation and emission spectra. The main spectroscopic parameters such as the  $g_2$  factor, the excitation and emission peaks of the red luminescence do not change. Thus, the internal structure of NBOHCs does not change even if with the neighbouring hydrogen interaction on NBOHCs. On the other hand, when the temperature increases from lower temperature to 200 K or above, all hydrogen in the silica glass will be dimerized, and the formed hydrogen molecule will be solidified in the glass [46]. If the temperature decreases from room temperature, the formerly solidified hydrogen will be gradually released into the glass network of silica. And if there is no negative center to attract the migrating hydrogen, they can act upon the NBOHC, resulting in the alteration of NBOHC.

In the case of the high-OH silica, these released hydrogen, including those interacted with NBOHCs, are attracted by the numerous hydroxyl groups. Consequently, the NBOHCs begin to lose their neighboring hydrogen from a temperature between 230 K and 150 K. As shown in Fig. 7, from 150 K to 78 K, all of NBOHCs exist as the state without neighboring hydrogen and its interaction. About the existence of metastable hydrogen-bonded hydroxyl groups [47], it was confirmed through photolysis experiments on the hydroxyl groups in silica [48].

In the case of the low-OH silica glass, most of the released hydrogen are not consumed by hydroxyl due to the absence of enough hydroxyl in the glass. Therefore, when the temperature is lowered down than 230 K, those NBOHCs without neighboring hydrogen are gradually altered to become the NBOHCs with neighboring hydrogen and its interaction. As shown in Fig. 8, at 78 K, the percentage of NBOHCs interacting with neighboring hydrogen increases to 95%. Although there is report that hydrogen begins to dimerize at the low temperature of 130 K [49], there is also reports that, even if the temperature drops to 30 K, hydrogen can still migrate in silica [46].

Further examination for the alteration process about two types of NBOHCs, as shown in Fig. 7 and Fig. 8, implies that the interaction between NBOHC and hydrogen is somewhat weaker and slower, compared with the interaction between hydroxyl group and hydrogen. As a result, although in the high-OH and low-OH silica glasses there exist different NBOHCs with and without neighbouring hydrogen interaction, they exhibit almost no change in the main  $g_2$  factor and the peak value of the red luminescence, only a slight but obvious change in the bandwidth of the EPR spectra as well as the excitation spectra and emission spectra. More importantly, such NBOHCs with and without neighbouring hydrogen interaction exhibit significant differences in the emission lifetime decay curves, especially at low temperature. It means that the decay of the red luminescence is sensitive to the alteration of the neighbouring environment close to NBOHCs, which is beneficial for the future more precise prediction of the laser induced damage of silica glasses.

#### 4. Conclusion

The NBOHCs generated in high-OH and low-OH silica glasses irradiated by gamma rays generally exhibit almost the same spectral characteristics at room temperature but some significantly different spectral characteristics at low temperature. Although the main  $g_2$ -factor is unchanged, the EPR spectra of NBOHC in high-OH silica glass show a little narrower bandwidth in the higher  $g$ -value range of the  $g_2$ -factor resonance absorption band. Although the emission peak is unchanged, the red luminescence spectra of NBOHC in high-OH silica glass show a little broader bandwidth in the higher energy side. And especially, the average emission lifetime of NBOHCs in high-OH silica glass is only ~8% higher than that in low-OH silica glass at room temperature, but it is ~130% higher at the low temperature of 78 K. These characteristics indicate that there exist two types of NBOHCs in silica. The first type is the NBOHC without neighboring hydrogen and its interaction, which corresponds to longer lifetime component and dominates in high-OH silica glass at lower temperature. The second type is the NBOHC with neighboring hydrogen

and its interaction, which corresponds to shorter lifetime component and dominates in low-OH silica glass at lower temperature. With the temperature decrease, the released hydrogen will be attracted by the large number of hydroxyl in the high-OH silica glass, forming metastable hydrogen-bonded hydroxyl and causing those NBOHCs that originally interacted with hydrogen to lose their interaction with hydrogen. On the other hand, there is not enough hydroxyl to attract the released hydrogen in the low-OH silica glass. Consequently, these released hydrogen only can interact with those NBOHCs originally without neighboring hydrogen. Due to the difference between NBOHCs with and without the interaction from neighboring hydrogen, small variations can be observed for high-OH and low-OH silica glasses even at room temperature. Such a variation will be magnified obviously at lower temperature since the percentages of longer and shorter lifetime components will differ greatly at lower temperature. Even if there is no transformation in the internal structure of NBOHCs, the effects without and with neighboring hydrogen as well as its interaction are evident in the emission lifetime decay curves of the red luminescence of the NBOHCs in silica glasses. If it is the case, the results and analysis about longer and shorter lifetime components of NBOHCs will be beneficial for a future comprehensive investigation on a more precise prediction for the laser-induced damage of silica. It is important to examine which one between these two lifetime components is responsible for laser induced damage of silica. More importantly, the variation in the emission lifetimes and decay curves of NBOHCs before and after damage, which can be highlighted with the temperature decrease, can reflect the change in the environment surrounding NBOHCs. Thus, the relations can be established between the laser induced damage of silica and the defects in silica, such as a certain type of NBOHC as well as other ions or defect centers close to or interacted with the NBOHC, which can be beneficial to reveal the source and even the precursor responsible for the laser induced damage of silica.

**Funding.** Bureau of International Cooperation, Chinese Academy of Sciences (23XH1248); Scientific and Innovative Action Plan of Shanghai (23ZR1471900).

**Disclosures.** The authors declare no conflicts of interest.

**Data availability.** Data underlying the results presented in this paper are not publicly available at this time but may be obtained from the authors upon reasonable request.

## References

1. L. A. Moore and C. M. Smith, "Fused silica as an optical material [Invited]," *Opt. Mater. Express* **12**(8), 3043–3059 (2022).
2. T. Liu, M. Zhu, W. Du, *et al.*, "A nodule dome removal strategy to improve the laser-induced damage threshold of coatings," *High Power Laser Sci. Eng.* **10**, e30 (2022).
3. R. K. Mark, L. B. Colin, and G. D. Stavros, "Luminescence investigation of SiO<sub>2</sub> surfaces damaged by 0.35-nm laser illumination," *Proc. SPIE* **3902**, 138–144 (2000).
4. R. K. Mark and G. D. Stavros, "Properties of modified silica detected within laser-induced damage sites," *Proc. SPIE* **4102**, 106–111 (2000).
5. J. Fournier, J. Néauport, P. Grua, *et al.*, "Luminescence study of defects in silica glasses under near-UV excitation," *Phys. Procedia* **8**, 39–43 (2010).
6. A. Beaudier, F. R. Wagner, and J.-Y. Natoli, "Using NBOHC fluorescence to predict multi-pulse laser-induced damage in fused silica," *Opt. Commun.* **402**, 535–539 (2017).
7. I. Bass, E. Feigenbaum, R. Raman, *et al.*, "Performance of multiple cone arrays as shadow cone blockers on NIF," *Proc. SPIE* **12300**, 33 (2022).
8. C. Lacombe, L. Lamagnère, G. Hallo, *et al.*, "Full-scale optic designed for onsite study of damage growth at the laser megajoule facility," *Opt. Express* **31**(3), 4291–4305 (2023).
9. L. Ying, L. Zheng-kun, Q. Ke-qiang, *et al.*, "Advances in large-aperture beam sampling gratings," *Optics and Precision Engineering* **24**, 2896–2901 (2016).
10. S. Borneis, T. Laštovička, M. Sokol, *et al.*, "Design, installation and commissioning of the ELI-Beamlines high-power, high-repetition rate HAPLS laser beam transport system to P3," *High Power Laser Sci. Eng.* **9**, e30 (2021).
11. A. Alessi, C. D'Amico, S. Girard, *et al.*, "Confocal-micro-luminescence characterization of femtosecond laser irradiated silica and borosilicate glasses," *Nucl. Instrum. Methods Phys. Res., Sect. B* **435**, 251–257 (2018).
12. Y. Liu, B. Liu, Y. Song, *et al.*, "Sub-30 fs Yb-fiber laser source based on a hybrid cascaded nonlinear compression approach," *Chin. Opt. Lett.* **20**, 100006 (2022).

13. B. Shen, H. Xiong, X. Zhang, *et al.*, "Post-treatment of 351 nm SiO<sub>2</sub> antireflective coatings for high power laser systems prepared by the sol-gel method," *Chin. Opt. Lett.* **20**(1), 011601 (2022).
14. C. Bouyer, R. Parreault, N. Roquin, *et al.*, "Impact of temporal modulations on laser-induced damage of fused silica at 351 nm," *High Power Laser Sci. Eng.* **11**, e15 (2023).
15. M. Xu, F. Shi, L. Zhou, *et al.*, "Investigation of laser-induced damage threshold improvement mechanism during ion beam sputtering of fused silica," *Opt. Express* **25**(23), 29260–29271 (2017).
16. Y. Zhong, F. Shi, Y. Tian, *et al.*, "Detailed near-surface nanoscale damage precursor measurement and characterization of fused silica optics assisted by ion beam etching," *Opt. Express* **27**(8), 10826–10838 (2019).
17. L. Skuja, "The origin of the intrinsic 1.9 eV luminescence band in glassy SiO<sub>2</sub>," *J. Non-Cryst. Solids* **179**, 51–69 (1994).
18. L. Skuja and A. Naber, "Laser-induced luminescence in glassy SiO<sub>2</sub> and neutron-irradiated alpha-quartz: three types of non-bridging oxygen hole centers," *Mater. Sci. Forum* **239–241**, 25–28 (1997).
19. L. Skuja, T. Suzuki, and K. Tanimura, "Site-selective laser-spectroscopy studies of the intrinsic 1.9-eV luminescence center in glassy SiO<sub>2</sub>," *Phys. Rev. B* **52**(21), 15208–15216 (1995).
20. J. C. Lagomacini, D. Bravo, M. León, *et al.*, "EPR study of gamma and neutron irradiation effects on KU1, KS-4 V and Infrasil 301 silica glasses," *J. Nucl. Mater.* **417**(1-3), 802–805 (2011).
21. L. Skuja, K. Kajihara, M. Hirano, *et al.*, "Oxygen-excess-related point defects in glassy/amorphous SiO<sub>2</sub> and related materials," *Nucl. Instrum. Methods Phys. Res., Sect. B* **286**, 159–168 (2012).
22. D. L. Griscom and E. J. Friebele, "Fundamental radiation-induced defect centers in synthetic fused silicas: Atomic chlorine, delocalized E' centers, and a triplet state," *Phys. Rev. B* **34**(11), 7524–7533 (1986).
23. J. C. Lagomacini, D. Bravo, A. Martín, *et al.*, "Growth kinetics of AlOHC defects in  $\gamma$ -irradiated silica glasses," *J. Non-Cryst. Solids* **403**, 5–8 (2014).
24. J. C. Lagomacini, D. Bravo, P. Martín, *et al.*, "EPR study of new defects in neutron irradiated KS-4 V and KU1 fused silica," *IOP Conf. Ser.: Mater. Sci. Eng.* **15**, 012052 (2010).
25. D. Bravo, J. C. Lagomacini, M. León, *et al.*, "Comparison of neutron and gamma irradiation effects on KU1 fused silica monitored by electron paramagnetic resonance," *Fusion Eng. Des.* **84**(2-6), 514–517 (2009).
26. Y. Sakurai and K. Nagasawa, "Radial distribution of some defect-related optical absorption and PL bands in silica glasses," *J. Non-Cryst. Solids* **277**(2-3), 82–90 (2000).
27. T. Mohanty, N. C. Mishra, S. V. Bhat, *et al.*, "Dense electronic excitation induced defects in fused silica," *J. Phys. D: Appl. Phys.* **36**(24), 3151–3155 (2003).
28. Y. Hayashi, Y. Okuda, H. Mitera, *et al.*, "Formation of drawing- or radiation-induced defects in germanium-doped silica core optical fiber," *Jpn. J. Appl. Phys.* **33**(2B), L233 (1994).
29. D. L. Griscom and M. Mizuguchi, "Determination of the visible range optical absorption spectrum of peroxy radicals in gamma-irradiated fused silica," *J. Non-Cryst. Solids* **239**(1-3), 66–77 (1998).
30. Y. Inaki, H. Yoshida, T. Yoshida, *et al.*, "Active Sites on Mesoporous and Amorphous Silica Materials and Their Photocatalytic Activity: An Investigation by FTIR, ESR, VUV–UV and Photoluminescence Spectroscopies," *J. Phys. Chem. B* **106**(35), 9098–9106 (2002).
31. H. Imai, K. Arai, H. Hosono, *et al.*, "Dependence of defects induced by excimer laser on intrinsic structural defects in synthetic silica glasses," *Phys. Rev. B* **44**(10), 4812–4818 (1991).
32. L. Skuja, "Optically active oxygen-deficiency-related centers in amorphous silicon dioxide," *J. Non-Cryst. Solids* **239**(1-3), 16–48 (1998).
33. Q. Jianbe, M. Akio, U. Takashi, *et al.*, "Ultrashort-pulse-laser-induced fine structure in synthetic fused silicas," *Proc. SPIE* **5350**, 281–288 (2004).
34. L. Vaccaro, M. Cannas, and R. Boscaino, "Phonon coupling of non-bridging oxygen hole center with the silica environment: Temperature dependence of the 1.9 eV emission spectra," *J. Lumin.* **128**(7), 1132–1136 (2008).
35. A. Anedda, G. Bongiovanni, M. Cannas, *et al.*, "A 1.9 eV photoluminescence induced by 4 eV photons in high-purity wet synthetic silica," *J. Appl. Phys.* **74**(11), 6993–6995 (1993).
36. Y. Kawaguchi and S. Yamamoto, "Mechanically and optically stimulated luminescence spectra of silica glass: the role of defects on photoradiation," *Radiat. Prot. Dosim.* **65**(1), 409–412 (1996).
37. J. Zhou and B. Li, "Origins of a damage-induced green photoluminescence band in fused silica revealed by time-resolved photoluminescence spectroscopy," *Opt. Mater. Express* **7**(8), 2888–2898 (2017).
38. J. Qian, G. Wang, D. Shen, *et al.*, "Tunable point defects in hydroxyl fused silica enabled by ultrashort laser pulses: photostimulated luminescence and functional module fabrication," *Opt. Mater. Express* **10**(5), 1241–1248 (2020).
39. L. Skuja, K. Tanimura, and N. Itoh, "Correlation between the radiation-induced intrinsic 4.8 eV optical absorption and 1.9 eV photoluminescence bands in glassy SiO<sub>2</sub>," *J. Appl. Phys.* **80**(6), 3518–3525 (1996).
40. N. Ollier, K. Piven, C. Martinet, *et al.*, "Impact of glass density on the green emission and NBOHC formation in silica glass: A combined high pressure and 2.5 MeV electron irradiation," *J. Non-Cryst. Solids* **476**, 81–86 (2017).
41. L. Vaccaro, M. Cannas, and V. Radzig, "Luminescence properties of nonbridging oxygen hole centers at the silica surface," *J. Non-Cryst. Solids* **355**(18-21), 1020–1023 (2009).
42. Y. Sakurai, "Oxygen-related red photoluminescence bands in silica glasses," *J. Non-Cryst. Solids* **316**(2-3), 389–392 (2003).
43. Y. Sakurai, K. Nagasawa, H. Nishikawa, *et al.*, "Characteristic red photoluminescence band in oxygen-deficient silica glass," *J. Appl. Phys.* **86**(1), 370–373 (1999).

44. Y. Sakurai, "Effect of thermal heat treatment on oxygen-deficiency-associated defect centers: Relation to 1.8 eV photoluminescence bands in silica glass," *J. Appl. Phys.* **95**(2), 543–545 (2004).
45. Y. Guyot, A. Steimacher, M. P. Belançon, *et al.*, "Spectroscopic properties, concentration quenching, and laser investigations of Yb<sup>3+</sup>-doped calcium aluminosilicate glasses," *J. Opt. Soc. Am. B* **28**(10), 2510–2517 (2011).
46. K. Kajihara, L. Skuja, M. Hirano, *et al.*, "Diffusion and Reactions of Hydrogen in F<sub>2</sub>-Laser-Irradiated SiO<sub>2</sub> Glass," *Phys. Rev. Lett.* **89**(13), 135507 (2002).
47. M. Mizuguchi, L. Skuja, H. Hosono, *et al.*, "Photochemical processes induced by 157-nm light in H<sub>2</sub>-impregnated glassy SiO<sub>2</sub>:OH," *Opt. Lett.* **24**(13), 863–865 (1999).
48. K. Kajihara, L. Skuja, M. Hirano, *et al.*, "Formation and decay of nonbridging oxygen hole centers in SiO<sub>2</sub> glasses induced by F<sub>2</sub> laser irradiation: In situ observation using a pump and probe technique," *Appl. Phys. Lett.* **79**(12), 1757–1759 (2001).
49. D. L. Griscom, "Defect structure of glasses: Some outstanding questions in regard to vitreous silica," *J. Non-Cryst. Solids* **73**(1-3), 51–77 (1985).